Tunneling Planar Hall Effect in Topological Insulators: Spin-Valves and Amplifiers

Benedikt Scharf,[1] Alex Matos-Abiague,[1] Jong E. Han,[1] Ewelina M. Hankiewicz,[2] and Igor Žutić[1]

[1]*Department of Physics, University at Buffalo, State University of New York, Buffalo, NY 14260, USA*
[2]*Institute for Theoretical Physics and Astrophysics, University of Würzburg, Am Hubland, 97074 Würzburg, Germany*

(Dated: January 7, 2016)

We investigate tunneling across a single ferromagnetic barrier on the surface of a three-dimensional topological insulator. In the presence of a magnetization component along the bias direction, a tunneling planar Hall conductance (TPHC), transverse to the applied bias, develops. Electrostatic control of the barrier enables a giant Hall angle, with the TPHC exceeding the longitudinal tunneling conductance. By changing the in-plane magnetization direction it is possible to change the sign of both the longitudinal and transverse differential conductance without opening a gap in the topological surface state. The transport in a topological insulator/ferromagnet junction can thus be drastically altered from a simple spin-valve to an amplifier.

PACS numbers: 73.43.Jn,85.75.-d,73.43.Qt,73.50.Jt

Exotic properties of three-dimensional topological insulators (3D TIs) arise from their helical surface states in which electrons are described as 2D Dirac fermions with spin-momentum locking [1]. Unlike graphene, TIs have large spin-orbit coupling (SOC) leading to striking manifestations of the conservation of angular momentum from a colossal Kerr rotation [2] and control of photocurrents [3] to robust magnetization switching [4].

The interplay between magnetism and SOC in ferromagnet(F)/TI junctions provides a versatile platform to study fundamental effects and spintronic applications [1, 4]. Previous tunneling studies have largely focused on the longitudinal response [5–7]. Intuitively, transport across the barrier should be dominated by the normal incidence. Hence, a common expectation in tunnel junctions is that the transverse (Hall) response is negligible, especially for an in-plane magnetization.

In contrast to previous manifestations of the Hall effect, such as the anomalous [8, 9], tunneling anomalous [10, 11], and planar Hall effects [12], we propose an unexplored tunneling planar Hall effect (TPHE) mechanism emerging in F/TI junctions (see Fig. 1), qualitatively different from these manifestations in terms of the relevant geometry and the magnetization configuration. In particular, the proposed effect is maximized for a planar magnetization parallel to the applied bias, where these other Hall effects vanish [13].

Unlike in conventional tunneling, a thick barrier with TIs can still lead to a large conductance due to Klein tunneling [13]. We show that an asymmetry in the tunneling conductance due to the in-plane barrier magnetization enables efficient transverse (Hall) spin-valves. Furthermore, with spin-momentum locking and a tunable resonant transmission, these spin-valves can also display a *transverse* negative differential (ND) conductance even in the limit of vanishing applied bias, suggesting a path to amplifiers and other active spintronic devices [14].

This peculiar behavior arises from asymmetric tunnel-

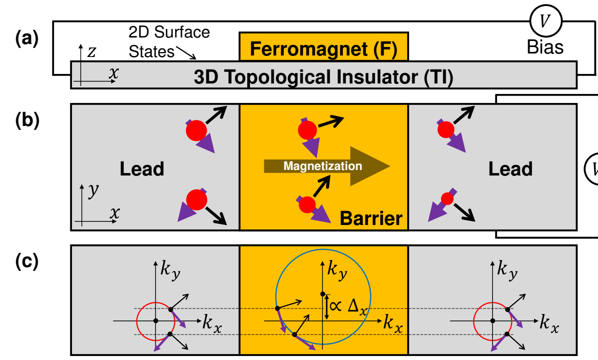

FIG. 1. (Color online) (a) Schematic setup. (b) Origin of the planar Hall conductance and net Hall voltage, V_H, due to asymmetric tunneling. The circle sizes represent the asymmetry in transmission probabilities arising from the interfacial mismatch of spin directions (locked to the velocity). (c) Spin mismatch: Fermi circles in the TI (upper Dirac cone) and the barrier (lower Dirac cone, shifted by a proximity-induced exchange splitting Δ_x). In (b) and (c) violet (black) arrows denote the electron spin orientation (direction of motion).

ing of electrons with opposite incident angles through the barrier as shown in Fig. 1(b). The finite tunneling planar Hall conductance (TPHC) can be understood as the spin mismatch between TI and F selecting electrons with positive transverse velocity [15] to be transmitted more effectively [Fig. 1(b)]. The interfacial spin mismatch results from spin-momentum locking and a shift of the Dirac cone due to the exchange splitting [Fig. 1(c)]. Translational symmetry along the y-axis yields an effective Snell's law [16] preserving the transverse momentum, while the longitudinal momentum changes sign on the lower Dirac cone (the group velocity points to its apex, see Ref. 13).

Our system is described by the effective Hamiltonian

$$\hat{H}_0 = v_{\mathrm{F}} \left(\boldsymbol{\sigma} \times \hat{\boldsymbol{p}}\right) \cdot \boldsymbol{e}_z + \left(V_0 - \boldsymbol{\Delta} \cdot \boldsymbol{\sigma}\right) h(x) \qquad (1)$$

with the barrier function $h(x) = \Theta(-x)\Theta(x+d)$ for a square (finite) barrier of width d and $h(x) = d\delta(x)$ for the respective δ-barrier. Here, v_F is the Fermi velocity of the surface states ($v_\mathrm{F} \approx 6\times10^5$ m/s in Bi_2Se_3 [17]), $\hat{\boldsymbol{p}}$ and $\boldsymbol{\sigma}$ denote vectors containing the momentum operators and Pauli spin matrices [1], while $\boldsymbol{\Delta}$ and V_0 describe the proximity-induced ferromagnetic exchange splitting and an electrostatic potential barrier, respectively. A planar exchange field $\boldsymbol{\Delta}$ shifts the apex of the Dirac cones from the origin to $(-\Delta_y/\hbar v_\mathrm{F}, \Delta_x/\hbar v_\mathrm{F})^T$ in the $k_x k_y$-plane. Therefore, for $\Delta_y = 0$ the longitudinal (transverse) transport is even (odd) in Δ_x.

The conductance for a bias along the x-direction is obtained from the eigenstates of Eq. (1) with energy E and conserved momentum $\hbar k_y$ [see Fig. 1(c)], $\Psi_{k_y}(x,y) = \exp(\mathrm{i}k_y y)\Phi(x)/\sqrt{2S}$ with the surface area S and

$$\Phi(x) = \begin{cases} \chi_+ \mathrm{e}^{\mathrm{i}k_x x} + r_\mathrm{e}\chi_- \mathrm{e}^{-\mathrm{i}k_x x}, & x < -d, \\ l\tilde{\chi}_+ \mathrm{e}^{\mathrm{i}\tilde{k}_+ x} + m\tilde{\chi}_- \mathrm{e}^{\mathrm{i}\tilde{k}_- x}, & -d < x < 0, \\ t_\mathrm{e}\chi_+ \mathrm{e}^{\mathrm{i}k_x x}, & x > 0 \end{cases} \tag{2}$$

for the finite barrier. For the δ-barrier, the states $\Phi(x<0)$ and $\Phi(x>0)$ are given by the first and third lines of Eq. (2), respectively. Defining the angle $-\pi/2 \leq \theta \leq \pi/2$ as $\hbar v_\mathrm{F} k_x = |E|\cos\theta$ and $\hbar v_\mathrm{F} k_y = |E|\sin\theta$, the momenta are given by $\hbar v_\mathrm{F}\tilde{k}_\pm = -\Delta_y \pm \hbar v_\mathrm{F}\tilde{k}_x$ and the spinors by $\chi_\pm = (1, b_\pm)^T$ and $\tilde{\chi}_\pm = (1, \tilde{b}_\pm)^T$ with $b_\pm = \mp\mathrm{i}\,\mathrm{sgn}(E)\mathrm{e}^{\pm\mathrm{i}\theta}$, $\tilde{b}_\pm = \left[(|E|\sin\theta - \Delta_x) \mp \mathrm{i}\hbar v_\mathrm{F}\tilde{k}_x\right]/(E - V_0 - \Delta_z)$, and

$$\hbar v_\mathrm{F}\tilde{k}_x(E,\theta) = \sqrt{(E-V_0)^2 - (\Delta_x - |E|\sin\theta)^2 - \Delta_z^2}. \tag{3}$$

Carefully invoking the boundary conditions [13, 18] to determine r_e, t_e, l, m in Eq. (2) yields the transmission

$$T(E,\theta) = \frac{1}{1 + \frac{(V_0\,\mathrm{sgn}(E)\sin\theta - \Delta_x)^2 + \Delta_z^2\cos^2\theta}{(\hbar v_\mathrm{F}/d)^2\cos^2\theta}\frac{\sin^2 Z_\mathrm{eff}}{Z_\mathrm{eff}^2}}, \tag{4}$$

where $Z_\mathrm{eff} = \tilde{k}_x(E,\theta)d$ for a finite barrier and $Z_\mathrm{eff} = \sqrt{V_0^2 - \Delta^2}\,d/(\hbar v_\mathrm{F})$ for a δ-barrier with $\Delta = \sqrt{\Delta_x^2 + \Delta_z^2}$. Here, $T(E,\theta)$ is independent of Δ_y and asymmetric with respect to θ for finite Δ_x.

We focus on the case $\Delta = |\Delta_x|$, $\Delta_z = 0$, while the effects of finite Δ_z are discussed in Ref. 13. The transmission from Eq. (4) displays two qualitatively different regimes: (i) oscillatory, with real Z_eff as a consequence of Klein tunneling in Dirac systems like graphene [19], and (ii) decaying, with complex Z_eff and typical for massive low-energy systems described by Schrödinger's equation. A remarkable property of our system is that by controlling the magnetization and/or the top gate potential (recall Z_eff depends on V_0 and Δ) it is possible to switch between the two regimes and produce very large differences in $T(E,\theta)$.

Such a tunable transmission can lead to a large anisotropy for some incident angles. In the oscillatory

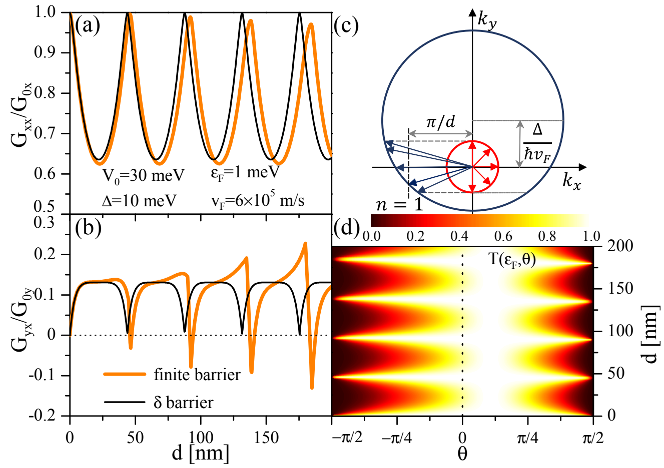

FIG. 2. (Color online) Dependence of the (a) longitudinal and (b) transverse conductances on d for finite and δ-barriers. (c) Fermi circles in the leads (inner circle) and barrier (outer circle). The arrows denote the wave vectors of states with positive x-component of the velocity and the vertical dashed line indicates the first-order resonance condition. (d) Transmission $T(\varepsilon_\mathrm{F},\theta)$ of a finite barrier as a function of d and θ.

regime, in particular, we find from Eq. (4) that perfect transmission is realized for

$$V_0\,\mathrm{sgn}(E)\sin\theta = \Delta \quad \text{or} \quad Z_\mathrm{eff}(E,\theta) = n\pi, \quad n = 1, 2, \ldots \quad . \tag{5}$$

Here, the first equality describes perfect transmission at each interface due to the absence of any spin mismatch between TIs and F. The second equality is a resonance condition for constructive interference when a multiple of the longitudinal wavelength $2\pi/\tilde{k}_x$ matches d [20].

Using Eq. (4), the tunneling conductance at zero temperature, for a bias applied in the x-direction, reads as

$$G_{xx/yx} = \frac{e^2}{h}\frac{|\varepsilon_\mathrm{F}|D_{x/y}}{2\pi\hbar v_\mathrm{F}}\int_{-\pi/2}^{\pi/2} \mathrm{d}\theta\, T(\varepsilon_\mathrm{F},\theta)\left\{\begin{array}{l}\cos\theta \\ \mathrm{sgn}(\varepsilon_\mathrm{F})\sin\theta\end{array}\right., \tag{6}$$

where $D_{x/y}$ is the width perpendicular to the current flow in the x/y-direction and -e is the electron charge. We normalize $G_{xx/yx}$ to the Sharvin conductance (transparent barrier), $G_{0x/y} = (e^2/h)\,|\varepsilon_\mathrm{F}|\,D_{x/y}/(\pi\hbar v_\mathrm{F})$ [21].

For a δ-barrier and $|V_0| \gg \Delta$, Eq. (4) can be expanded up to the lowest order in Δ/V_0,

$$G_{xx}/G_{0x} \approx \sec^2 Z_0 - \tanh^{-1}|\cos Z_0|\tan^2 Z_0/|\cos Z_0|, \tag{7}$$

$$G_{yx}/G_{0y} \approx (\pi\Delta/2V_0)\,|\sin Z_0|\,(1 - |\sin Z_0|)^2/\cos^4 Z_0, \tag{8}$$

where $Z_0 = V_0 d/(\hbar v_\mathrm{F})$ [22]. These expressions capture the oscillatory behavior of $G_{xx/yx}$ and reveal that at the resonance condition, $Z_\mathrm{eff} \approx Z_0 = n\pi$, $G_{xx} = G_{0x}$ reaches perfect transmission, whereas G_{yx} vanishes. Such a qualitative behavior is corroborated by the full δ-barrier dependence of $G_{xx/yx}$ on d, shown in Figs. 2(a) and (b).

Even though the δ-barrier provides a good approximation for small d, it fails to describe intriguing effects, such as the appearance of negative values of G_{yx} and the increase of its amplitude with d. Hence, we will focus on the finite barrier and employ the δ-model only to obtain analytical approximations.

The main features observed in Figs. 2(a) and (b) can be understood by analyzing the phase space available for tunneling shown in Fig. 2(c) for $V_0 > \varepsilon_\mathrm{F} > 0$. Here, the inner (outer) circle with radius $|\varepsilon_\mathrm{F}|/(\hbar v_\mathrm{F})$ $[|V_0 - \varepsilon_\mathrm{F}|/(\hbar v_\mathrm{F})]$ represents the k-space Fermi circle in the leads (barrier) and the arrows indicate the Fermi wave vectors of the scattering states available for transport. As discussed in Fig. 1, the asymmetry between the scattering states with $k_y > 0$ $(0 < \theta < \pi/2)$ and $k_y < 0$ $(-\pi/2 < \theta < 0)$ due to Δ causes a finite TPHC. For illustration, we show in Fig. 2(d) the transmission, $T(\varepsilon_\mathrm{F}, \theta)$, of a finite barrier as a function of d and θ. The asymmetry of $T(\varepsilon_\mathrm{F}, \theta)$ with respect to $\theta = 0$ due to the first equality in Eq. (5) can clearly be seen, which results in the appearance of a nonzero G_{yx} after the integration in Eq. (6). On the other hand, the oscillatory behavior with d in Fig. 2(d) is governed by $\sin^2 Z_\mathrm{eff}$ in Eq. (4).

When $|V_0 - \varepsilon_\mathrm{F}| > \Delta + |\varepsilon_\mathrm{F}|$, the Fermi circle of the leads is inside that of the barrier as shown in Fig. 2(c). Then, for each Fermi vector in the leads, there is one available in the barrier and the system is purely in the Klein tunneling regime. The deviations between the finite and δ-barrier models with increasing d originate from the angular dependence of Z_eff and the ensuing asymmetric resonances in the case of a finite barrier, explained by Fig. 2(c): With increasing d, the first-order resonance $[n = 1$ in Eq. (5)$]$ starts to move towards smaller k_x-values and, at $d \approx 46$ nm, it starts to cross the Fermi circle of the barrier. The first states reaching the resonance are those with $k_y > 0$, causing an increase in G_{yx} compared to the δ-barrier model. As d is further increased, the resonance moves to states with $k_y < 0$ producing a fast decrease in G_{yx}, which, eventually, becomes negative. In thicker barriers, the trend repeats periodically with d each time a new resonance becomes relevant. This occurrence of multiple resonances ($n = 1, 2$, etc) results in the increase of the amplitude of the TPHC for even larger values of d (if $|\varepsilon_\mathrm{F}| \ll |V_0|$) as shown in Fig. 2(b).

The interplay between V_0 and Δ and the appearance of a TPHC are illustrated by Fig. 3 for both (a) G_{xx} and (b) G_{yx} as well as (c) their ratio for a finite barrier with $d = 50$ nm and a fixed ε_F. Figures 3(a) and (b) clearly show the transition from a region of oscillatory Klein tunneling ($|V_0| > \Delta + 2\varepsilon_\mathrm{F} \approx \Delta$) to a region of decaying tunneling ($|V_0| < \Delta$). Such a transition can be understood by resorting to the analysis of the Fermi circles. As discussed above, the scheme in Fig. 2(b) corresponds to the Klein tunneling regime, but increasing Δ will shift up the Fermi circle of the barrier, which at $\Delta = V_0 - 2\varepsilon_\mathrm{F}$ starts to cross the Fermi circle of the

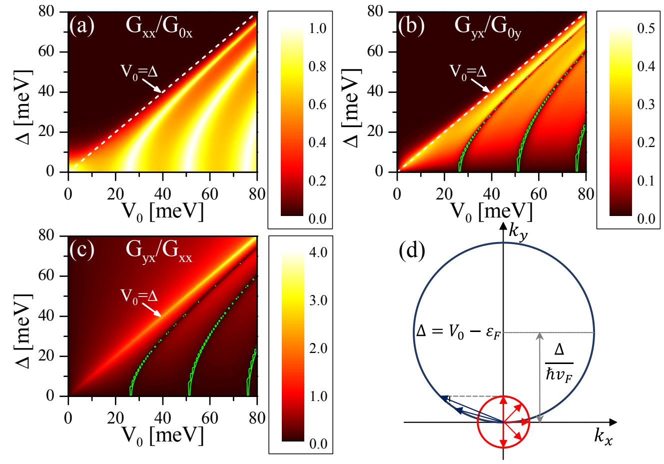

FIG. 3. (Color online) Dependence of the (a) longitudinal and (b) transverse conductances as well as (c) of their ratio on V_0 and Δ for a finite barrier with $d = 50$ nm, $\varepsilon_\mathrm{F} = 1$ meV, and $v_\mathrm{F} = 6.0 \times 10^5$ m/s. Green lines denote the boundaries of regions with negative conductance. (d) Same as in Fig. 2(c), but for larger Δ.

leads. Therefore, increasing Δ above that value results in the formation of an intermediate regime in which only a part of the available states can undergo Klein tunneling, while the other experiences decaying tunneling. The contrast between the two tunneling mechanisms becomes extreme when $\Delta = V_0 - \varepsilon_\mathrm{F}$. In such a situation, as shown in Fig. 3(d), Klein tunneling occurs only for states with $k_y > 0$, while those with $k_y < 0$ undergo decaying tunneling. This strong asymmetry in the tunneling favors the transmission of states with larger k_y values and results in a remarkably large ratio between the TPHC and the longitudinal conductance. As shown in Fig. 3(c), such a ratio can even exceed 1, implying large Hall angles, $\theta_\mathrm{H} = \arctan(G_{yx}/G_{xx}) \approx 75°$ for the parameters chosen here. Such giant values of the Hall angle are comparable to those recently detected in a 3D magnetic TI [23]. Green lines in Figs. 3(b) and (c) indicate negative values of the TPHC, whose origin is the same as in Fig. 2(c).

The δ-barrier model enables us to obtain an analytical expression for the giant Hall angle. Indeed, for $|V_0| \approx \Delta$,

$$G_{xx}/G_{0x} = \left[(2\ln|Z_0| - 1)\, Z_0^2 + 1\right] / \left(Z_0^2 - 1\right)^2, \quad (9)$$

$$G_{yx}/G_{0y} = \pi|Z_0| / \left[2\left(|Z_0| + 1\right)^2\right]. \quad (10)$$

Assuming $D_x = D_y$, we obtain

$$\tan\theta_\mathrm{H} = \frac{G_{yx}}{G_{xx}} = \frac{\pi|Z_0|\left(|Z_0| - 1\right)^2}{2\left[(2\ln|Z_0| - 1)\, Z_0^2 + 1\right]}, \quad (11)$$

which increases with $|Z_0|$, even though G_{xx} and G_{yx} individually decrease.

We next examine the current-voltage (I-V) characteristics and reveal the appearance of a negative differential

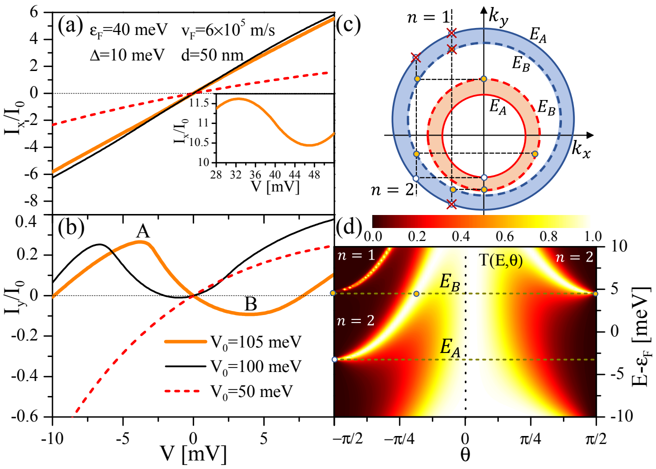

FIG. 4. (Color online) Bias dependence of the (a) longitudinal and (b) transverse currents for a finite barrier and different V_0. Assuming $D_x = D_y = 10$ μm, both currents are given in units of $I_0 = 12$ μA. (c) Same as in Fig. 2(c), but with thickened Fermi circles accounting for a finite energy window around $\varepsilon_{\rm F}$. (d) Transmission $T(E, \theta)$ for $V_0 = 105$ meV. The inset in (a) shows the appearance of a ND longitudinal conductance for $V_0 = 105$ meV at high bias voltages.

(ND) conductance. A ND longitudinal conductance observed in single barrier graphene transistors [24] appears also in our system as shown in the inset of Fig. 4(a). This occurs when the Fermi level in one lead is aligned with the Dirac point of the other lead. The size of the ND longitudinal conductance can be enlarged by scatterers in the tunneling barrier region [24]. Surprisingly, the transverse current, I_y, also shows a change of sign in its slope [segment from A to B in Fig. 4(b)], the signature of a ND Hall conductance (NDHC) [25], but within an operational range in which the differential longitudinal conductance remains positive [see Fig. 4(a)].

The appearance of a NDHC is exemplified for $V_0 = 105$ meV in Fig. 4(b) with the corresponding transmission coefficient $T(E, \theta)$ displayed in Fig. 4(d). Here, the key observation is that in the Klein tunneling regime, the asymmetry of the resonances with respect to $\theta = 0$ depends on the energy. Indeed, as depicted in Fig. 4(d), for different energies the resonances appear in the region $k_y < 0$, or $k_y > 0$, or in both. This behavior is explained in Fig. 4(c), where the Fermi circles of the leads and barrier have been thickened in order to account for the energy window from E_A (solid circles) to E_B (dashed circles) around the Fermi energy, $\varepsilon_{\rm F} = 40$ meV. The vertical lines marked by $n = 1$ and $n = 2$ indicate the resonance condition $Z_{\rm eff}(k_x, k_y) = n\pi$ as in Eq. (5). Open and full (yellow) dots represent the resonances seen in Fig. 4(d) at E_A and E_B, while crossed dots represent resonances forbidden by the conservation of k_y. The nonmonotonic behavior of the I_y-V characteristic in Fig. 4(b) follows from the positions of the resonances: The local maximum A emerges as the relevant energy window between $\varepsilon_{\rm F}$ and $\varepsilon_{\rm F} + eV$ starts to cross the resonance at E_A for a $k_y < 0$ [Figs. 4(c) and (d)] resulting in a reduced I_y with increasing V. This resonance is compensated for as another resonance favoring $k_y > 0$ is reached at E_B [Figs. 4(c) and (d)], giving rise to the local minimum B and subsequent increase of I_y in Fig. 4(b).

As shown in Fig. 4(b), the NDHC present for $V_0 = 100$ meV and $V_0 = 105$ meV is suppressed at $V_0 = 50$ meV, suggesting the possibility of controlling the NDHC by gate-tuning the barrier. Moreover, the I_y-V characteristic for $V_0 = 105$ meV resembles that of a typical active ND resistor, which is unusual for tunneling systems [26].

Despite the simplicity of a single ferromagnetic region, our system exhibits a variety of functionalities expected to require more complex spintronic devices [27, 28]. In addition to a spin-valve operation for magnetic sensing and storing information, shown in Figs. 4(a) and (b), positive, negative, and ND conductances can be tuned by properly adjusting the barrier potential, suitable for processing information. Such different resistive behaviors in the same system are attractive for potential applications in reconfigurable devices operating as feedback oscillators, active filters, modulators, and amplifiers [29]. These functionalities can be alternated both by the barrier potential and in a nonvolatile way using the magnetization orientation.

Our findings, expressed using Bi_2Se_3 parameters, could also be detected in other 3D topological insulators [1]. The appearance of a giant transverse response would support the expected topological character among an increasingly large class of materials [30]. To realize magnetic proximity effects for the in-plane transport, ferromagnetic insulators are desirable. This would preclude current flow in the more resistive ferromagnetic region [see Fig. 1(a)] and minimize hybridization with the topological insulator to enable a gate-tunable proximity-induced exchange splitting in the 2D surface states.

In addition to Eu-based materials [31], ferromagnet/topological insulator junctions could attain a higher temperature range by using Fe-enhanced magnetic proximity effects in (Bi,Mn)Te [32]. Employing yttrium iron garnet/$(Bi,Sb)_2Te_3$ junctions for an independent tuning of electronic properties and proximity-induced magnetism in topological insulators, observed up to 150 K [33], is a promising path to implement our proposal. A future work on the effects proposed here could involve studying the role of phonons, especially surface phonons, which have been shown to profoundly affect transport in topological insulators such as Bi_2Se_3 [34].

Acknowledgments. This work was supported by U.S. DOE, Office of Science BES, under Award DESC0004890 (A.M.-A., I.Ž.), by U.S. ONR N000141310754 (B.S.), the German Science Foundation (DFG) Grant No. SCHA 1899/1-1 (B.S.), and DFG Grant No. HA 5893/4-1 within SPP 1666 (E.M.H.).

[1] M. Z. Hasan and C. L. Kane, Rev. Mod. Phys. **82**, 3045 (2010); X.-L. Qi and S.-C. Zhang, Rev. Mod. Phys. **83**, 1057 (2011); S.-Q. Shen, *Topological insulators: Dirac equation in condensed matters* (Springer, Berlin, 2012).

[2] R. Valdés Aguilar, A. V. Stier, W. Liu, L. S. Bilbro, D. K. George, N. Bansal, L. Wu, J. Cerne, A. G. Markelz, S. Oh, and N. P. Armitage, Phys. Rev. Lett. **108**, 087403 (2012).

[3] J. W. McIver, D. Hsieh, H. Steinberg, P. Jarillo-Herrero, and N. Gedik, Nat. Nanotechnol. **7**, 96 (2012).

[4] A. Mellnik, J. Lee, A. Richardella, J. Grab, P. Mintun, M. Fischer, A. Vaezi, A. Manchon, E.-A. Kim, N. Samarth, and D. Ralph, Nature **511**, 449 (2014); Y. Fan, P. Upadhyaya, X. Kou, M. Lang, S. Takei, Z. Wang, J. Tang, L. He, L.-T. Chang, M. Montazeri, G. Yu, W. Jiang, T. Nie, R. N. Schwartz, Y. Tserkovnyak, and K. L. Wang, Nat. Mater. **13**, 699 (2014).

[5] Z. Wu, F. M. Peeters, and K. Chang, Phys. Rev. B **82**, 115211 (2010); Z. Wu and J. Li, Nanoscale Res. Lett. **7**, 90 (2012).

[6] X. Li, X. Duan, and K. W. Kim, Phys. Rev. B **89**, 045425 (2014); C. H. Li, O. M. J. van t Erve, J. T. Robinson, Y. Liu, L. Li, and B. T. Jonker, Nat. Nanotechnol. **9**, 218 (2014).

[7] J. Tian, I. Childres, H. Cao, T. Shen, I. Miotkowski, and Y. P. Chen, Solid State Commun. **191**, 1 (2014); J. Tian, I. Miotkowski, S. Hong, and Y. P. Chen, Sci. Rep. **5**, 14293 (2015).

[8] N. A. Sinitsyn, J. Phys. Condens. Matter **20**, 023201 (2008); N. Nagaosa, J. Sinova, S. Onoda, A. H. MacDonald, and N. P. Ong, Rev. Mod. Phys. **82**, 1539 (2010).

[9] D. Culcer and S. Das Sarma, Phys. Rev. B **83**, 245441 (2011).

[10] A. Vedyayev, N. Ryzhanova, N. Strelkov, and B. Dieny, Phys. Rev. Lett. **110**, 247204 (2013); A. V. Vedyayev, M. S. Titova, N. V. Ryzhanova, M. Y. Zhuravlev, and E. Y. Tsymbal, Appl. Phys. Lett. **103**, 032406 (2013).

[11] A. Matos-Abiague and J. Fabian, Phys. Rev. Lett. **115**, 056602 (2015); T. H. Dang, H. Jaffrès, T. L. Hoai Nguyen, and H.-J. Drouhin, Phys. Rev. B **92**, 060403 (2015).

[12] H. X. Tang, R. K. Kawakami, D. D. Awschalom, and M. L. Roukes, Phys. Rev. Lett. **90**, 107201 (2003); K. M. Seemann, F. Freimuth, H. Zhang, S. Blügel, Y. Mokrousov, D. E. Bürgler, and C. M. Schneider, Phys. Rev. Lett. **107**, 086603 (2011).

[13] For details see the Supplemental Material.

[14] I. Žutić, J. Fabian, and S. Das Sarma, Rev. Mod. Phys. **76**, 323 (2004); J. Fabian, A. Matos-Abiague, C. Ertler, P. Stano, and I. Žutić, Acta Phys. Slov. **57**, 565 (2007).

[15] In Fig. 1, we discuss the regime of $V_0 > \varepsilon_{\mathrm{F}} > 0$. Our arguments, however, are also valid for other regimes.

[16] I. Žutić and O. T. Valls, Phys. Rev. B **61**, 1555 (2000).

[17] H. Zhang, C.-X. Liu, X.-L. Qi, X. Dai, Z. Fang, and S.-C. Zhang, Nat. Phys. **5**, 438 (2009); D. Kim, S. Cho, N. P. Butch, P. Syers, K. Kirshenbaum, S. Adam, J. Paglione, and M. S. Fuhrer, Nat. Phys. **8**, 459 (2012).

[18] A. Matos-Abiague and K. A. Kouzakov, Phys. Rev. A **68**, 017401 (2003).

[19] M. I. Katsnelson, K. S. Novoselov, and A. K. Geim, Nat. Phys. **2**, 620 (2006); S. Bhattacharjee and K. Sengupta, Phys. Rev. Lett. **97**, 217001 (2006); J. Linder and A. Sudbø, Phys. Rev. Lett. **99**, 147001 (2007).

[20] While the first condition is only valid for $\Delta_z = 0$ and $|V_0| > |\Delta_x|$, the second condition given by Eq. 5 is also valid for $\Delta_z \neq 0$.

[21] I. Žutić and S. Das Sarma, Phys. Rev. B **60**, R16322 (1999).

[22] For $\Delta_z \neq 0$, Δ is replaced by Δ_x in Eq. (8).

[23] A. Kandala, A. Richardella, S. Kempinger, C.-X. Liu, and N. Samarth, Nat. Comm. **6**, 7434 (2015).

[24] L. Britnell, R. V. Gorbachev, A. K. Geim, L. A. Ponomarenko, A. Mishchenko, M. T. Greenaway, T. M. Fromhold, K. S. Novoselov, and L. Eaves, Nat. Comm. **4**, 1794 (2013).

[25] Unrelated to Hall phenomena, that is, in the absence of magnetization and magnetic fields, a finite transverse negative resistance was reported in n-type Ge [M. Shyam and H. Kroemer, Appl. Phys. Lett. **12**, 283 (1968); C. Hammar, Phys. Rev. B **4**, 2560 (1971)].

[26] Typically, resonant tunneling devices exhibit I-V characteristics of passive ND resistors, where the ND conductance region does not cross the origin.

[27] S. Maekawa, S. Valenzuela, S. E., and E. Kimura, T., *Spin Current* (Oxford University, New York, 2012).

[28] J. Wunderlich, B.-G. Park, A. C. Irvine, L. P. Zarbo, E. Rozkotova, P. Nemec, V. Novak, J. Sinova, and T. Jungwirth, Science **330**, 1801 (2010).

[29] R. L. Boylestad and L. Nashelsky, *Electronic Devices and Circuit Theory, Eleventh Edition* (Prentice Hall, 2012).

[30] W. Feng, D. Xiao, J. Ding, and Y. Yao, Phys. Rev. Lett. **106**, 016402 (2011).

[31] M. Li, C.-Z. Chang, B. J. Kirby, M. E. Jamer, W. Cui, L. Wu, P. Wei, Y. Zhu, D. Heiman, J. Li, and J. S. Moodera, Phys. Rev. Lett. **115**, 087201 (2015).

[32] I. Vobornik, U. Manju, J. Fujii, F. Borgatti, P. Torelli, D. Krizmancic, Y. S. Hor, R. J. Cava, and G. Panaccione, Nano Lett. **11**, 4079 (2011).

[33] Z. Jiang, C.-Z. Chang, C. Tang, P. Wei, J. S. Moodera, and J. Shi, Nano Lett. **15**, 5835 (2015).

[34] M. V. Costache, I. Neumann, J. F. Sierra, V. Marinova, M. M. Gospodinov, S. Roche, and S. O. Valenzuela, Phys. Rev. Lett. **112**, 086601 (2014).